

Article

A PET Fluorescent Probe for Dynamic Pd²⁺ Tracking with Imaging Applications in the Nanofiber and Living Cells

Zhao Cheng ^{1,*} , Xilang Jin ², Yinggang Liu ² and Xuejiao Zhang ¹¹ School of Pharmacy, Xi'an Medical University, Xi'an 710021, China² School of Materials and Chemical Engineering, Xi'an Technological University, Xi'an 710032, China

* Correspondence: chengzhao@xiyi.edu.cn

Abstract: Constructed on the moiety of a lactam screw ring, a near-infrared fluorescent probe RCya for Pd²⁺ was designed under the PET mechanism and synthesized by incorporating 2,4-dihydroxybenzaldehyde as the recognition group. Dynamic detection of aqueous Pd²⁺ by the probe RCya could be accomplished through ion competition, linear response, fluorescence-pH/time stabilities, and other optical tests. Moreover, the high selectivity, low cytotoxicity, cell permeability, and lysosome accumulation properties of RCya enabled the imaging applications on solid-state RCya-PAN composite nanofibers and in living cells. The recognition mechanism of probe RCya toward Pd²⁺ was further studied through simulation calculation and MS analysis.

Keywords: palladium ion; imaging; nanofiber; cytotoxicity; mechanism

1. Introduction

Palladium, as a mature and early-used platinum-group catalyst, has a wide distribution in the soil, water, and other environmental sources. When entering the food chain through contaminated food or water and being taken into the human bodies, the food-borne intake palladium would not only accumulate in the organs but bound with thio-containing amino acids, proteins, DNA, and other related biomolecules [1], disrupting a variety of biological processes as a biological participant. For its toxicity, allergenicity, carcinogenicity, and therapeutic and biological effects [2,3], effective and quantitative methods for low-level and intracellular palladium detections are urgently needed. Moreover, ppm analytical accuracy should be achieved in the palladium detections, considering the proposed dietary palladium intake of 1.5–15 µg per person per day and the 5–10 ppm governmental regulations on palladium in end products/drugs [4].

Compared with the instrumental analyses with complex requirements on instruments and sample preparations, optical detection approaches, especially the colorimetric and fluorimetric analytical approaches [5,6], demonstrated unique advantages in low cost, simple operation, high sensitivity, and so on. However, most optical detections were reported to happen in the aqueous environment and required a good solubility of the related fluorescence probe. For more convenience and more future applications in target detection, more visualized detection methods between the probe and the target, such as naked-eye mode [7], solid-state detection, and dynamic imaging [8], should be adopted in the structural design of fluorescent probes.

Accordingly, a near-infrared fluorescent probe RCya for Pd²⁺ was synthesized by introducing the recognition group 2,4-dihydroxybenzaldehyde into the moiety of a lactam screw ring [9]. In an aqueous environment, probe RCya demonstrated specific responses toward Pd²⁺ over other metals, accompanied by a good quantitative relationship, good fluorescence-pH/time stabilities, and remarkable changes in UV-Vis/fluorescence spectra of RCya-Pd²⁺. Besides the dynamic Pd²⁺ detection in aqueous solutions, colorimetric and specific detection of Pd²⁺ by RCya could also be accomplished on solid-state RCya-PAN



Citation: Cheng, Z.; Jin, X.; Liu, Y.; Zhang, X. A PET Fluorescent Probe for Dynamic Pd²⁺ Tracking with Imaging Applications in the Nanofiber and Living Cells. *Molecules* **2023**, *28*, 3065. <https://doi.org/10.3390/molecules28073065>

Academic Editor: Haiying Liu

Received: 27 February 2023

Revised: 27 March 2023

Accepted: 28 March 2023

Published: 29 March 2023



Copyright: © 2023 by the authors. Licensee MDPI, Basel, Switzerland. This article is an open access article distributed under the terms and conditions of the Creative Commons Attribution (CC BY) license (<https://creativecommons.org/licenses/by/4.0/>).

composite nanofibers. Furthermore, MTT and bioimaging in living cells indicated the low cytotoxicity, good cell permeability, and lysosome accumulation properties of probe RCya, enabling the dynamic labeling and tracking of Pd²⁺ for instant and time-lapse imaging in biological applications, also predicting the probe's future applications as real-time detection methods for Pd²⁺ in clinical diagnosis.

2. Results

2.1. Structural Characterization

With a four-step synthetic route, the fluorescent probe RCya for Pd²⁺ was synthesized. Structures of RCya and related intermediates were characterized by ¹H NMR and HRMS. The calculation and measurement results of MS were all matched, and characteristic ¹H NMR chemical shifts were all located at the reasonable ppm range and in accordance with the target structures.

2.2. Spectroscopic Properties

2.2.1. Selectivity and Competition

A specific detection for biological Pd²⁺, for palladium ions' complex ions coexistence environment, is a difficult issue, and the parameters of selectivity/competition must be taken into consideration.

For the detection of aqueous Pd²⁺, the selectivity of probe RCya toward Pd²⁺ was evaluated in PBS buffer solution (EtOH : H₂O = 1 : 99, pH = 7.4) with the concentration of RCya 10 μmol L⁻¹ and metal ions 40 μmol L⁻¹. When excited by 635 nm, probe RCya itself displayed maximal fluorescence intensity at 735 nm and maximal UV-Vis absorbance at 713 nm, respectively. Upon the addition of various metal ions, as illustrated in the front rows of Figure 1a,b, there were obvious differences in these RCya–metal ion systems, among which only Pd²⁺ immediately triggered a significant optical enhancement at 735 nm for fluorescence and 713 nm for UV-Vis, with nearly no interferences from other metal ions.

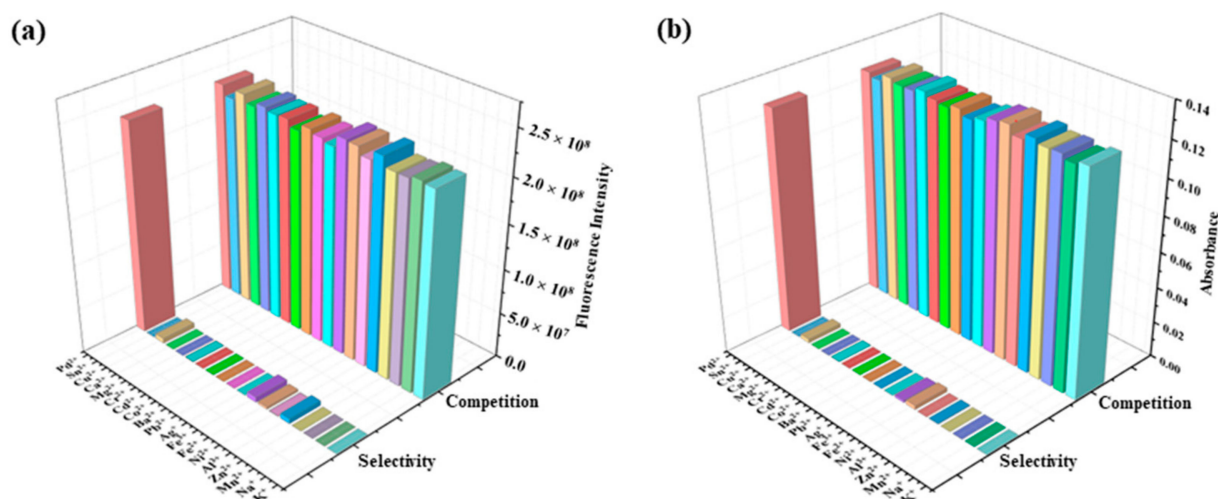


Figure 1. Selectivity and competition of RCya toward Pd²⁺ in Pd²⁺-competing ions coexisting systems at the excitation wavelength of 635 nm: (a) fluorescence intensity at 735 nm; and (b) UV-Vis absorbance at 713 nm of the probe and metal ion system. From left to right (bar 1–19): Pd²⁺; Sn²⁺; Cu²⁺; Ca²⁺; Mg²⁺; Cr³⁺; Cd²⁺; Co²⁺; Ba²⁺; Pb²⁺; Ag⁺; Fe³⁺; Fe²⁺; Ni²⁺; Al³⁺; Zn²⁺; Mn²⁺; Na⁺; and K⁺.

Subsequently, 40 μmol L⁻¹ Pd²⁺ was added to the front-row-represented RCya–metal ion solutions, resulting in ions coexistence systems of RCya–metal ion–Pd²⁺. From the systems of RCya–metal ion to RCya–metal ion–Pd²⁺, the resulting enhancements in 735 nm (fluorescence) and 713 nm (UV-Vis) peaks were depicted in the rear rows of Figure 1a,b. Compared with the front rows, it was undoubtedly the subsequently added Pd²⁺ that

induced significant increases in the RCya–metal ion–Pd²⁺ systems. Meanwhile, for every RCya–metal ion–Pd²⁺ system, optical intensities of 735 nm (fluorescence) and 713 nm (UV-Vis) were enhanced of almost the same fold, which meant every system's enhancement was caused by the addition of Pd²⁺, and the existence of other metal ions had nearly no competitions or influences on the specific optical responses of RCya–Pd²⁺.

The selectivity and competition tests showed that probe RCya was highly sensitive to Pd²⁺, predicting the future use of RCya for Pd²⁺ detection in complex environments, which will not be affected by the tested background of other metal ions.

2.2.2. Linear Relationship

For a better understanding of the quantitative relationship between probe RCya and Pd²⁺, fluorescence and UV-Vis titration experiments were performed with 10 μmol L⁻¹ RCya and 0.0–4.0 equiv. Pd²⁺ to RCya. As 0.0–4.0 equiv. Pd²⁺ was gradually added into RCya, a significant enhancement of RCya–Pd²⁺ located at 735 nm for fluorescence (Figure 2a) and 713 nm for UV-Vis absorbance (Figure 2b) resulted.

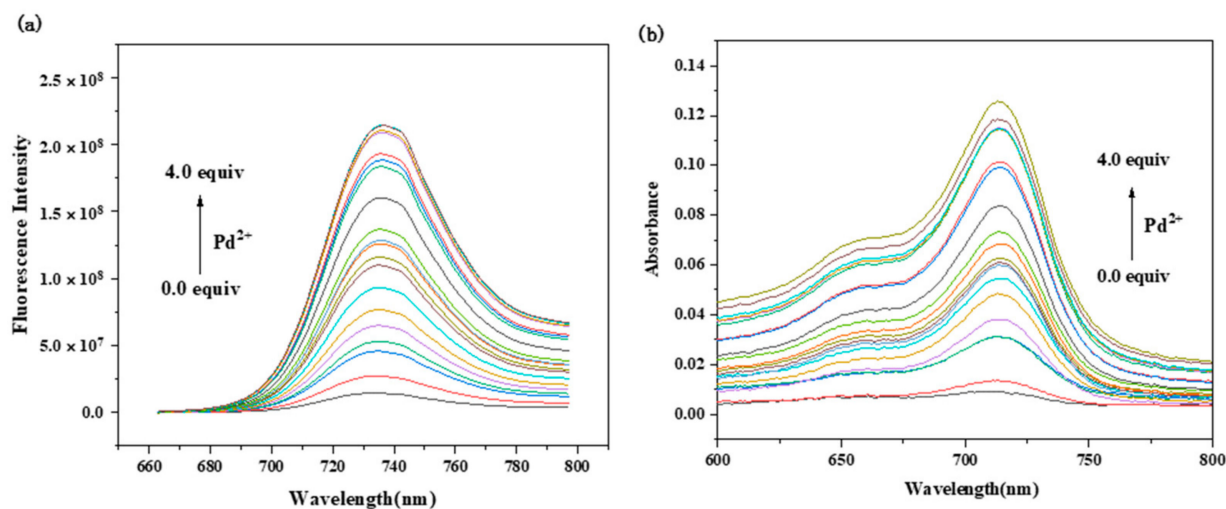


Figure 2. (a) Fluorescence and (b) UV-Vis spectra of probe RCya titrated with Pd²⁺ at the excitation wavelength of 635 nm (RCya: 10 μmol L⁻¹, Pd²⁺: 0.0–4.0 equiv. to RCya).

Analysis of the fluorescence spectra of RCya–Pd²⁺ resulted in a linear relationship of the fluorescence intensity of RCya versus [Pd²⁺] in the concentration range of 0–40 μmol L⁻¹ Pd²⁺ [10], with the linear equation seen in Figure 3a as $y = 2.00737 \times 10^7 + 5.58777 \times 10^6 x$ ($R^2 = 0.99622$) (y , I_{735} : fluorescence intensity of the RCya–Pd²⁺ system at the wavelength of 735 nm; x , [Pd²⁺]: the concentration of Pd²⁺), indicating a highly quantitative detection of Pd²⁺ by probe RCya. Furthermore, based on the fluorescence titration results and the formula for the limit of detection $LOD = 3\sigma/k$, the detection limit of Pd²⁺ by RCya could be determined. In the detection limit equation, the fluorescence emission spectra of RCya in the absence and presence of Pd²⁺ were measured three times, and the standard deviation of blank fluorescence measurement (σ in the detection limit equation) was obtained, whereas the slope k in the equation was calculated through the plot of fluorescence intensity at 735 nm versus Pd²⁺ concentration. The detection limit was calculated to be 0.362 μmol L⁻¹, indicating a high sensitivity of RCya toward Pd²⁺.

Similarly, the linear response of RCya's UV-Vis absorbance toward [Pd²⁺] (0–40 μmol L⁻¹) could be expressed by the following equation [11]: $y = 0.00292 x - 0.0122$ ($R^2 = 0.9943$) (y , Abs_{713} : UV-Vis absorbance of the RCya–Pd²⁺ system at the wavelength of 713 nm; x , [Pd²⁺]: the concentration of Pd²⁺), as depicted in Figure 3b.

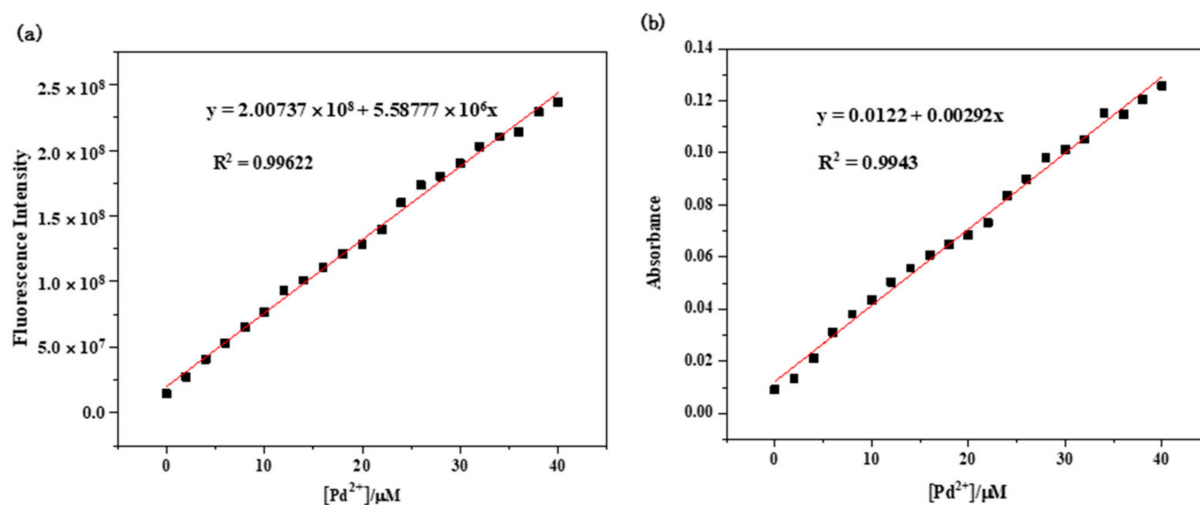


Figure 3. Linear relationships at the excitation wavelength of 635 nm: (a) fluorescence intensity at 735 nm of the RCya + Pd²⁺ system; (b) absorbance at 713 nm of the RCya + Pd²⁺ system.

2.2.3. Influence Parameters

For dynamic Pd²⁺ labeling and tracking in biological systems, fluorescence-time stabilities of the RCya–Pd²⁺ system should be analyzed to achieve dynamic and time-lapse detections. Initially, there underwent a recognition process of RCya and Pd²⁺ with a time length of about 40 s, (a) fluorescence intensity at 735 nm, and (b) UV-Vis absorbance at 713 nm, increasing gradually. After a response time of 0–40 s, optical intensities were then saturated and remained steady for minutes (Figure 4), indicating the probe RCya's not only instant but time-lapse fluorescence imaging applications for dynamic Pd²⁺ detections in biological systems.

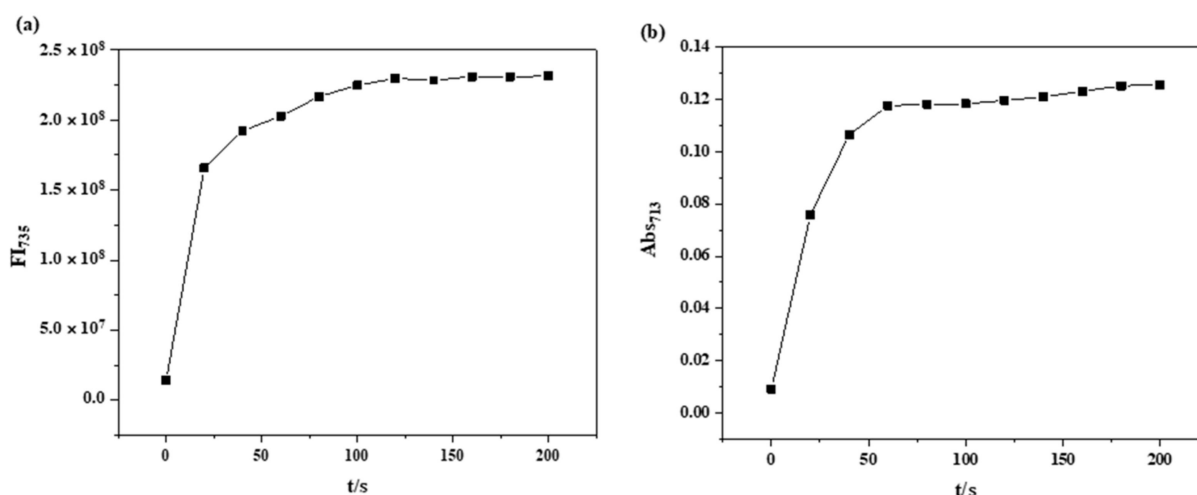


Figure 4. Time dependence of the RCya + Pd²⁺ system at the excitation wavelength of 635 nm: (a) fluorescence intensity at 735 nm versus time, (b) UV-Vis absorbance at 713 nm versus time (RCya: 10 $\mu\text{mol L}^{-1}$, Pd²⁺: 40 $\mu\text{mol L}^{-1}$).

When probe RCya was applied to Pd²⁺ detection in biological systems, fluorescence-pH stabilities of RCya and RCya + Pd²⁺ should also be examined for the complex and variable pH environment. In comparison with probe RCya's steady fluorescence intensity at 735 nm, as seen in Figure 5, at a varied pH region of 3.0 to 9.0, fluorescence intensity at 735 nm of RCya–Pd²⁺ initially kept relatively steady and gradually decreased (Figure 5), suggesting an appropriate pH range of 3.0–7.0 for Pd²⁺ detection by RCya, which will

satisfy most physiological pH environment for Pd^{2+} detections [12]. The differences between RCya and RCya + Pd^{2+} in fluorescence-pH stabilities could be explained by the recognition mechanism of RCya and Pd^{2+} . When probe RCya combined with Pd^{2+} , the probe's structure partly transformed, and the synthetic intermediate compound **3** was released. As a rhodamine derivative, compound **3** only gave off steady fluorescence signals at the acidic conditions, which was in accordance with the stabilities of RCya + Pd^{2+} at the pH range of 3.0–7.0. Once compound **3** was located in the basic environment, the rhodamine moiety became unstable, and its fluorescence dramatically decreased, consistent with the phenomenon of RCya + Pd^{2+} beyond pH = 7.

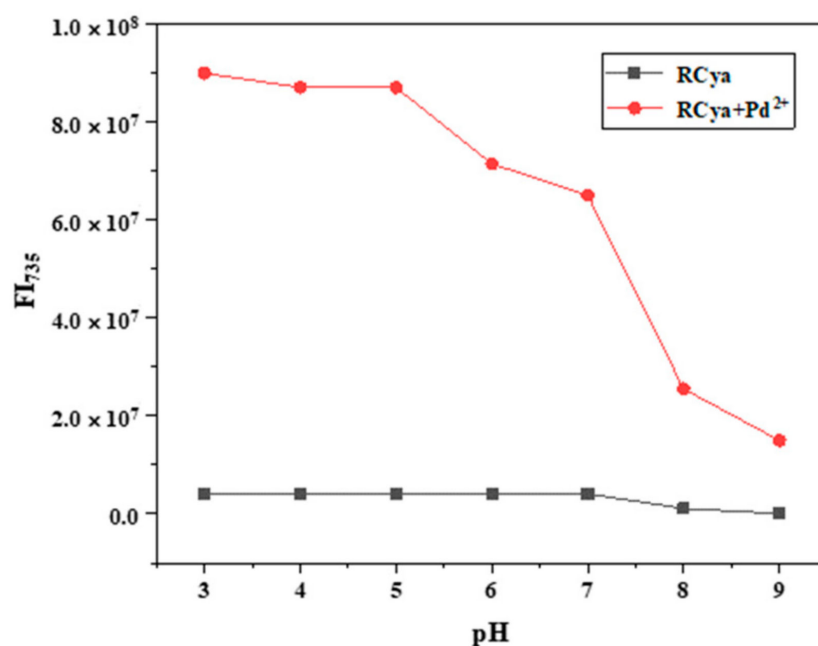


Figure 5. pH dependence of probe RCya in the absence and presence of Pd^{2+} .

2.3. Mechanism

2.3.1. Proposed Mechanism

Illustrated in Figures 1a and 2a and partly revealed by the fluorescence-pH stabilities of RCya and RCya + Pd^{2+} in Figure 5, before and after the combination of Pd^{2+} by RCya, the probe's structural transformation and the relevant changes in fluorescence signals, accompanied with a release of the rhodamine derivative compound **3**, could be inferred [13,14] (Figure 6).

Before the addition of Pd^{2+} into RCya, probe RCya, with a strong intramolecular PET process [15], only gave off a very weak fluorescence at 735 nm (Figure 1a); even when probe RCya was located at a varied pH region of 3.0 to 9.0 (Figure 5), the fluorescence emission kept steady due to its stable structure. When Pd^{2+} was added into RCya and the probe combined with Pd^{2+} , the amide carbonyl group of the probe coordinated with Pd^{2+} , and, thus, RCya- Pd^{2+} combined, the lactam ring in RCya was opened due to the formation of complex RCya- Pd^{2+} , which not only inhibited the PET process but emitted the specific rhodamine red fluorescence and the fluorescence emission intensity at 735 nm enhanced significantly (Figure 1a). Similarly, as 0.0–4.0 $\mu\text{mol L}^{-1}$ Pd^{2+} was gradually added into RCya, the processes of PET-off and rhodamine ring-opened moiety would intensify, corresponding to the gradual fluorescence enhancements at 735 nm in Figure 2a.

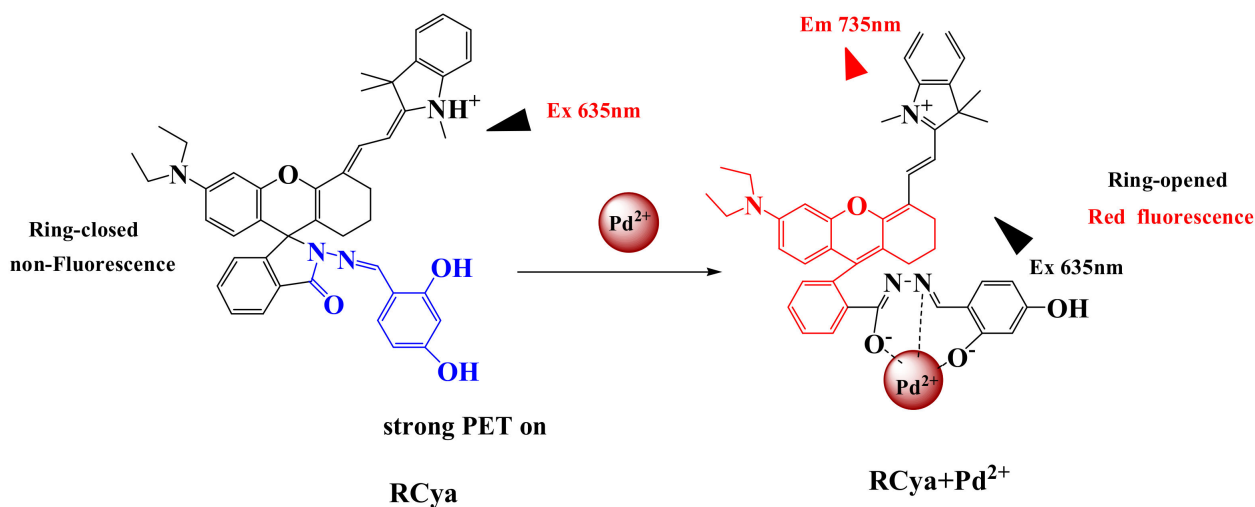
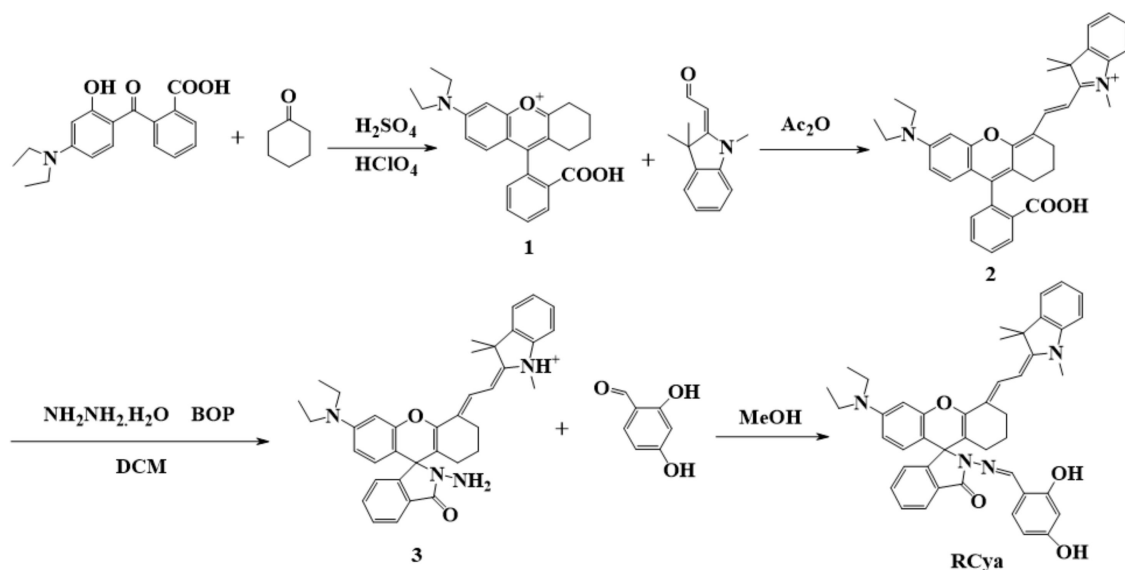


Figure 6. Proposed recognition mechanism of probe RCya to Pd²⁺.

Meanwhile, the combination process resulted in a ring-opened rhodamine moiety, which was highly similar to the synthetic intermediate compound 3 (Scheme 1), as illustrated in the proposed recognition mechanism of Figure 6.



Scheme 1. Synthetic route of probe RCya.

2.3.2. DFT Calculation

For an extended evaluation of the photo-induced luminescence process [16,17], DFT calculations were employed and performed using the Gaussian 09 program. With the molecular models constructed on the corresponding relations of 6–31G* for elements C and H, 6–31 + G* for elements N, O, and S, and DGDZVP for Pd, the simulated diagram for the theoretical photo-induced luminescence process before and after Pd²⁺ combination by RCya was illustrated in Figure 7, which provided sufficient information on HOMO–LUMO gaps, combination sites, and the chemical activation process, further confirming the proposed mechanism.

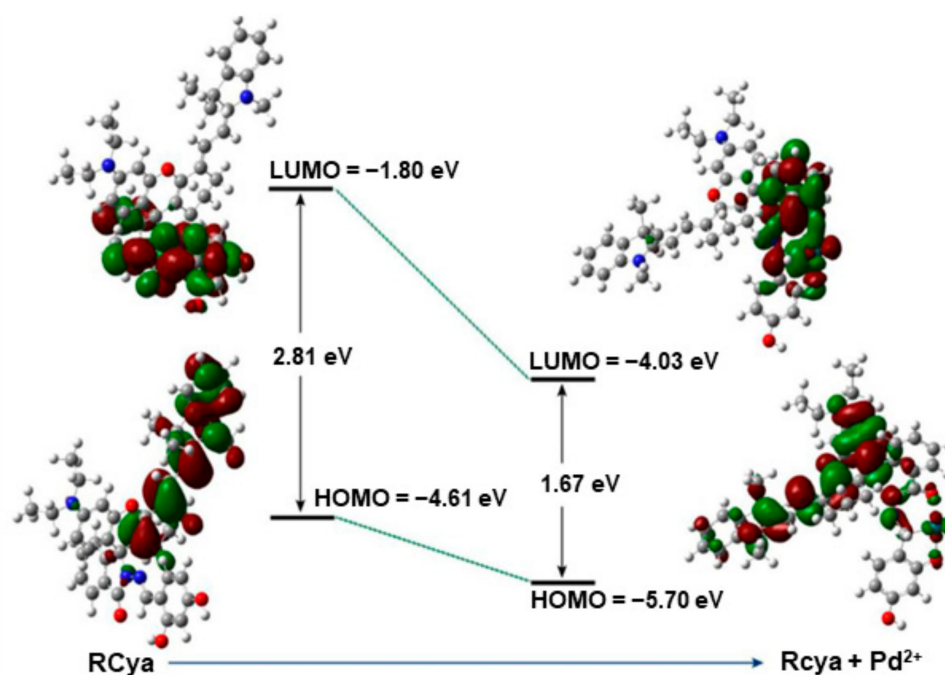


Figure 7. Density functional theory theoretical calculation for the combination of RCya and Pd²⁺.

In the free state of probe RCya, the HOMO and LUMO of RCya itself were located at the benzopyrrole fragment of the fluorophore and 2,4-dihydroxybenzaldehyde fragment of the recognition site, respectively. In comparison, the HOMO of the complex RCya–Pd²⁺ was distributed entirely along the fluorophore, and the LUMO was still mainly located at the recognition site. The separation of HOMO and LUMO means possibilities for probe RCya to be excited. Furthermore, the calculated HOMO–LUMO energy gap for probe RCya was 2.81 eV, with a much smaller value of 1.67 eV for complex RCya–Pd²⁺, indicating that the complex RCya–Pd²⁺ located at a lower energy level, the combination process of RCya and Pd²⁺ was accompanied by a shift from a high energy level of the reactant RCya itself to a lower one of the product RCya–Pd²⁺, enabling the resulting complex RCya–Pd²⁺ with more stabilities. Additionally, due to its lower energy level and more stabilities, the complex RCya–Pd²⁺ was much more easily excited than probe RCya and gave off a much stronger fluorescence emission, in accordance with the optical properties depicted in Figures 1 and 2.

2.3.3. MS Analysis

Apart from the theoretical calculations, a further HRMS analysis offered us more details concerning the structural transformation from probe RCya to coordination complex RCya–Pd²⁺. When Pd²⁺ was added into RCya and the complex RCya + Pd²⁺ formed, a diagnostic peak at $m/z = 559.2883$ was obtained (Figure 8b), which was very close to $m/z = 560.3299$ [compound 3 + H⁺] of the synthetic intermediate compound 3 (Figure 8c). Through the combination process of RCya and Pd²⁺, the target peak $m/z = 693.3237$ [RCya+H⁺] of probe RCya (Figure 8a) was shifted to $m/z = 559.2883$ for RCya + Pd²⁺ (Figure 8b), indicating that the fragment of 2,4-dihydroxybenzene was eliminated when the lactam ring of RCya opened to capture Pd²⁺ and, meanwhile, the structure of precursor compound 3 was given back. Finally, the processes of lactam ring-opening, Pd²⁺ combination, and 2,4-dihydroxybenzene elimination combined to induce the tested $m/z = 559.2883$ in Figure 8b, corresponding to the proposed mechanism in Figure 6.

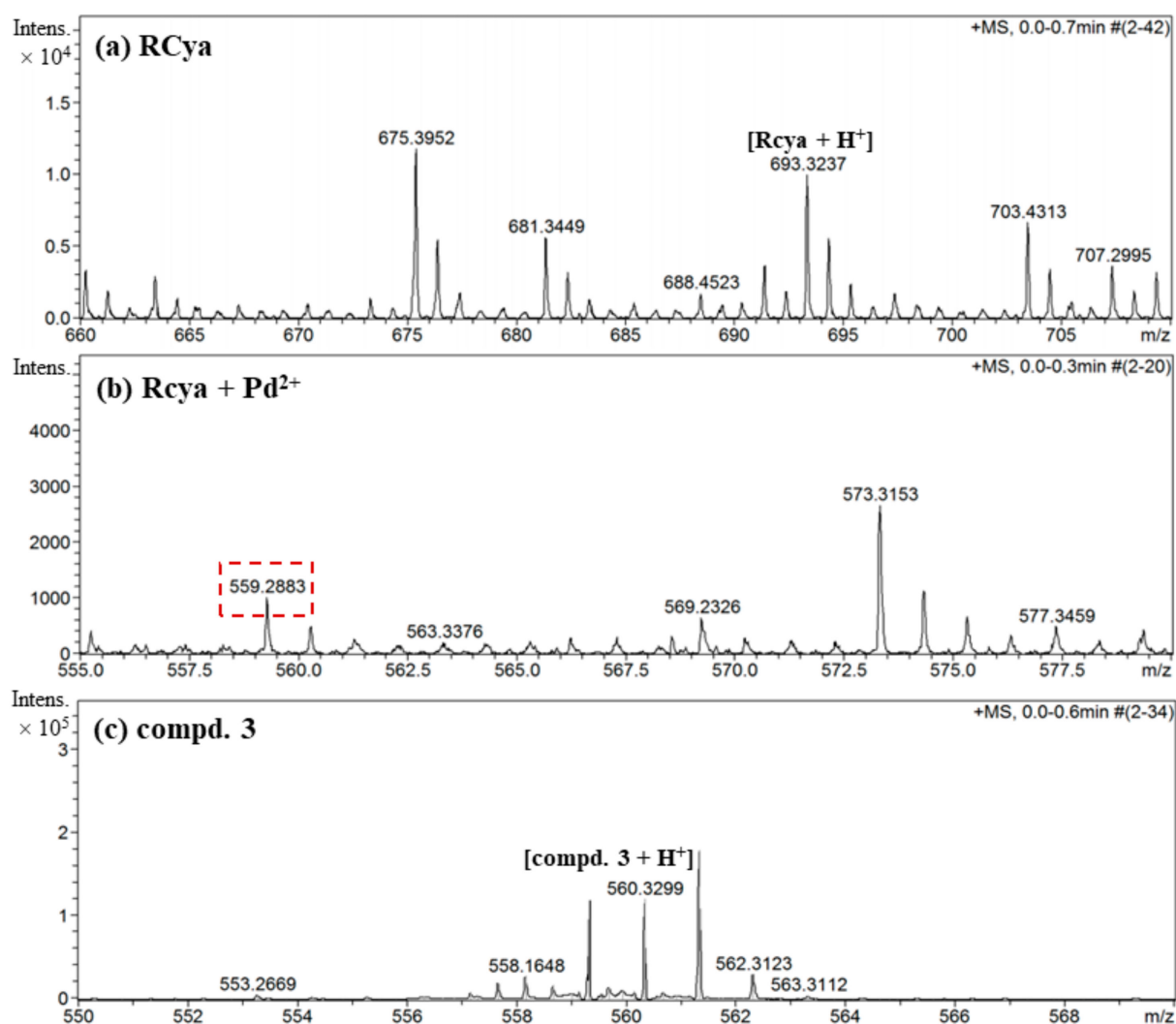


Figure 8. HRMS analysis on the recognition process of probe RCya to Pd²⁺.

2.4. Nanofiber Imaging Applications

For the detection and imaging of Pd²⁺ by RCya on solid-state, RCya–PAN composite nanofibers were prepared and immersed into Pd²⁺ (5.0 $\mu\text{mol L}^{-1}$)/other cations solution (100 $\mu\text{mol L}^{-1}$), respectively, then imaged under ambient light or under the 365 nm ultraviolet lamp (Figure 9). Not surprisingly, only Pd²⁺ induced a colorless-to-red colorimetric and light yellow-to-green fluorescence change, accomplishing a simultaneous naked-eye Pd²⁺ detection under ambient light and spectroscopic Pd²⁺ detection under a UV lamp.

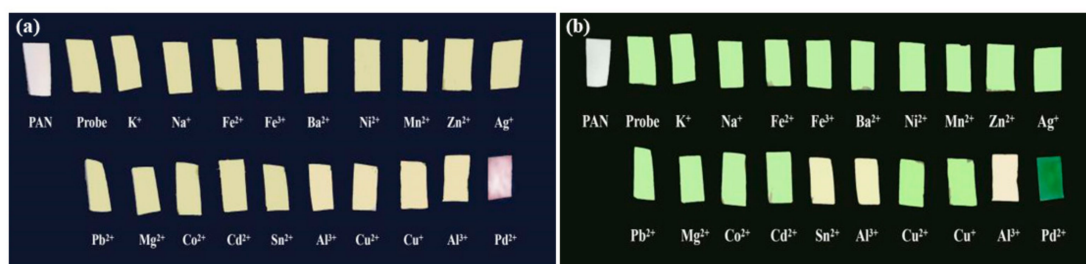


Figure 9. Photographs of RCya–PAN composite nanofibers upon exposure to the aqueous solutions of various metal ions: (a) under ambient light; (b) under a hand-held UV lamp at 365 nm.

2.5. MTT Assay

A standard MTT assay was performed with HeLa cells to evaluate the potential imaging and diagnostic applications [18,19] of probe RCya. MTT assay was performed in HeLa cells with a concentration gradient of 6.25, 12.50, 25.00, 50.00, and 100.00 $\mu\text{mol L}^{-1}$ for each group, respectively. The illustrations in Figure 10 indicated that there was no significant toxic effect of RCya on HeLa cells when incubated for 24 h. At the spectroscopic testing concentration of RCya (10 $\mu\text{mol L}^{-1}$), HeLa cell viability was about 95% for RCya, even when the concentration of RCya reached the highest 100 $\mu\text{mol L}^{-1}$ in MTT assay, the cytotoxicity of HeLa cells remained below 25%, indicating relatively low cytotoxicity of RCya at the concentration range of 0–100 $\mu\text{mol L}^{-1}$, which satisfies the cytotoxicity concentration demands of ppm/ $\mu\text{mol L}^{-1}$ Pd²⁺ distributions in most biological systems.

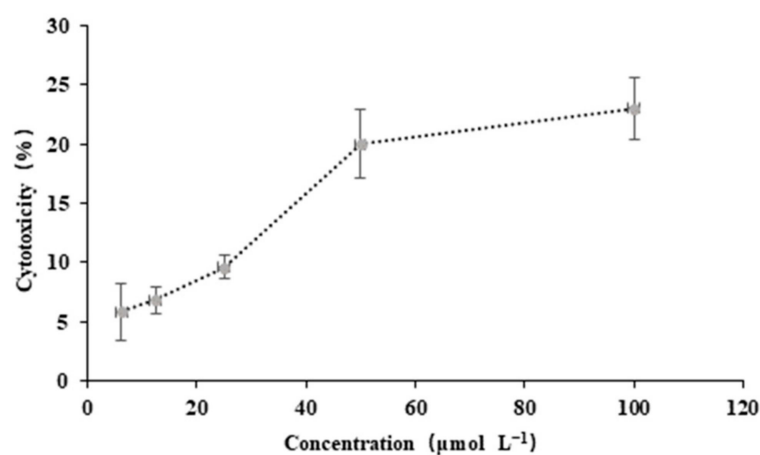


Figure 10. The cytotoxicity of RCya on HeLa at 24 h.

2.6. Bioimaging

As seen in Figure 11a, an initial 30 min incubation of HeLa and 10 $\mu\text{mol L}^{-1}$ RCya only gave off weak green fluorescence. When 40 $\mu\text{mol L}^{-1}$ Pd²⁺ was subsequently added in and RCya + Pd²⁺ was incubated with HeLa for another 2 h at 37 °C, in comparison with Figure 11a, bright and specific red fluorescence of the rhodamine moiety was emitted from the intracellular area (Figure 11c), demonstrating the recognition of added Pd²⁺ by RCya over a very short time. The overlay of the bright-field image (Figure 11b) and fluorescence image (Figure 11c) are shown in Figure 11d, which located the red fluorescence signals in the perinuclear region of the cytosol [20,21], indicating that probe RCya was cell permeable and could be applied to the dynamic imaging of Pd²⁺ in living cells [22].

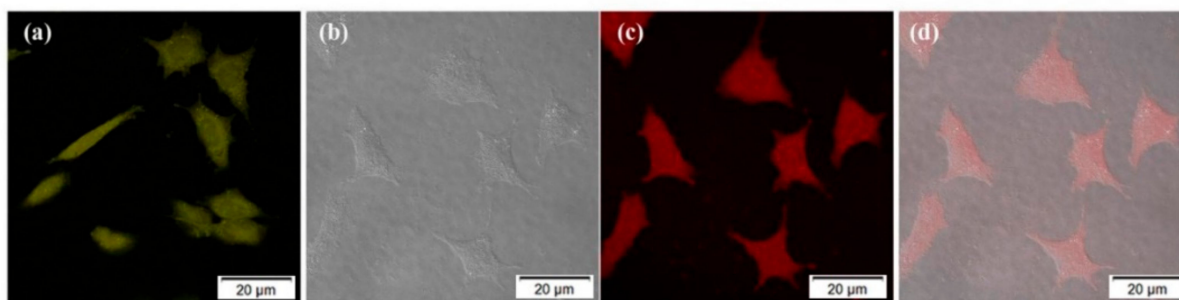


Figure 11. Bioimaging of probe RCya–Pd²⁺ in HeLa: (a) the fluorescent image of HeLa incubated with 10 $\mu\text{mol L}^{-1}$ RCya for 30 min; (b) a further incubation of (a) with 40 $\mu\text{mol L}^{-1}$ Pd²⁺ for another 2 h at bright field; (c) a further incubation of (a) with 40 $\mu\text{mol L}^{-1}$ Pd²⁺ for another 2 h at dark field; (d) an overlay of (b) and (c). Scale bar: 20 μm .

As implied by the bioimaging results in Figure 11, the accumulated areas of RCya in the cytoplasm were further analyzed in HeLa cells. By incorporating commercially available localization reagents Mito-Tracker Green (Mito) and Lyso-Tracker Green (Lyso), the co-staining experiments of RCya–Mito/Lyso were performed, and lysosome targeting properties of the synthesized RCya were revealed. As displayed in Figure 12a, RCya + Pd²⁺ and the lysosome-targeting reagent Lyso-Tracker Green demonstrated a good overlap, presenting large yellow patches. In contrast with Figure 12a, RCya + Pd²⁺ and the mitochondria-targeting reagent Mito-Tracker Green only gave a poor overlap, shown as the red/green patches in Figure 12b. Consequently, the co-staining imaging indicated that RCya could be used as an efficient lysosome-targetable probe for dynamic Pd²⁺ imaging in living cells, providing potential tools for monitoring the function of lysosomes in the autophagy processes.

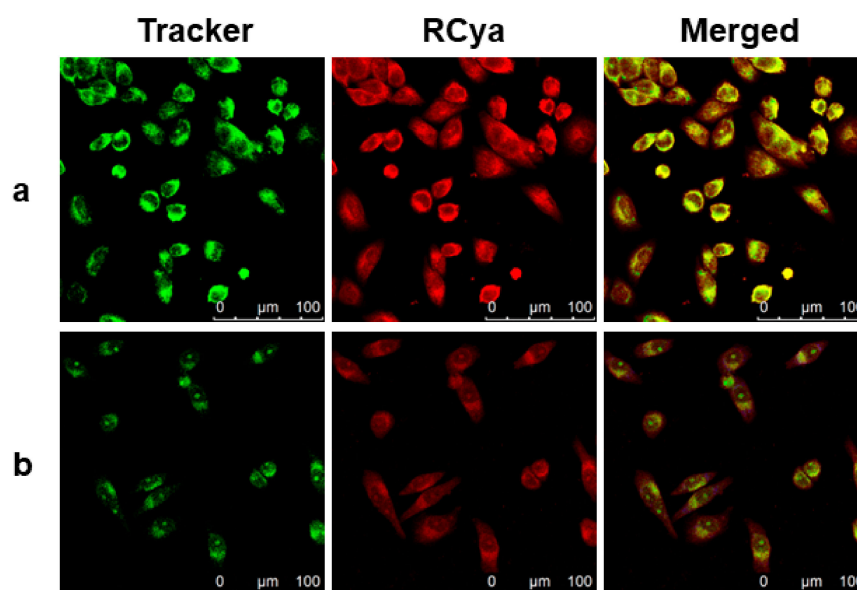


Figure 12. Con-staining fluorescence imaging of RCya + Pd²⁺ and organelle-targeting trackers in HeLa: (a) the fluorescent image of HeLa costained with 1 $\mu\text{mol L}^{-1}$ RCya, 1 $\mu\text{mol L}^{-1}$ Pd²⁺ and 100 nmol L^{-1} Lyso-Tracker Green; (b) the fluorescent image of HeLa costained with 1 $\mu\text{mol L}^{-1}$ RCya, 1 $\mu\text{mol L}^{-1}$ Pd²⁺ and 100 nmol L^{-1} Mito-Tracker Green. Red channel: $\lambda_{\text{ex}} = 559 \text{ nm}$, $\lambda_{\text{em}} = 688\text{--}788 \text{ nm}$. Green channel: $\lambda_{\text{ex}} = 488 \text{ nm}$, $\lambda_{\text{em}} = 511\text{--}539 \text{ nm}$.

3. Discussion

With the structure characterized by HRMS/¹H NMR and optical properties analyzed by UV-Vis/fluorescence imaging, a fluorescent probe RCya was proven quite useful for the dynamic detection of Pd²⁺ in the lysosomes in real time. On the one side, highly specific responses to Pd²⁺ over other metal ions were accomplished by the probe, and the detections of Pd²⁺ by RCya not only happened in aqueous solutions but on solid-state nanofibers and in living cells. On the other, the combination mechanism and structural transformation of probe RCya in the recognition process of Pd²⁺ were studied through DFT calculations and HRMS analysis, offering us sufficient information on the structural design of fluorescent probes in future research. Furthermore, RCya–Pd²⁺ demonstrated good fluorescence stability at a relatively wide physiological pH range and in a considerably great time span; also, RCya–Pd²⁺ showed low cytotoxicity, good cell permeability, and lysosome-targeted properties in the MTT assay and dynamic bioimaging, which, combined, could predict probe RCya be appropriate for the biological applications under complex environments.

4. Materials and Methods

4.1. Reagents and Equipment

^1H NMR spectra were recorded on a Varian INOVA-400 spectrometer at 400 MHz, and chemical shifts were reported relative to internal standard tetramethylsilane (TMS). MS analyses were carried out using Bruker micro TOF-Q II mass spectrophotometer. Fluorescent spectra were measured with a HITACHI F-4500 fluorescence spectrophotometer. UV-Vis spectra were measured on a SHIMADZU UV-2550 spectrometer. FT-IR spectra were recorded with KBr pellets on Bruker EQUINOX-55 FT-IR spectrometer. Results of cytotoxicity were analyzed with the Softmax pro software (version 2.2.1) in Spectra max190-Molecular devices. Cell-imaging experiments were performed using OLYMPUS FV1000 TY1318 laser scanning confocal microscope.

All the reagents and solvents used for synthesis were commercially available and used without further purification unless otherwise noted. Mito-Tracker Green, Lyso-Tracker Green, and HeLa cells were purchased from KeyGen BioTECH (Nanjing, China). The reaction process was monitored by thin-layer chromatography (TLC) on silica gel GF254. The products were purified by column chromatography on Merck silica gel (250–400 mesh ASTM). Phosphate Buffered Saline (PBS, pH = 7.4) was purchased from a Sinopharm chemical reagent company, Shanghai, China. Double-distilled water was used throughout the process of solution preparation and spectroscopic testing. Solutions of metal ions were prepared from their nitrate and chloride salts, PdCl_2 , SnCl_2 , CuCl_2 , MgCl_2 , $\text{Cr}(\text{NO}_3)_3$, CdCl_2 , CoCl_2 , BaCl_2 , PbCl_2 , AgNO_3 , FeCl_3 , FeCl_2 , NiCl_2 , AlCl_3 , ZnCl_2 , MnCl_2 , NaCl and KCl .

4.2. Synthesis

By introducing 2,4-dihydroxybenzaldehyde as the recognition group into the moiety of a lactam screw ring [23,24], a near-infrared fluorescent probe, RCya for Pd^{2+} , was synthesized, as shown in Scheme 1. Structures of the intermediates were characterized by IR, ^1H NMR, and HRMS; their optical properties and the recognition mechanism of probe RCya were further confirmed by UV-Vis, HRMS, DFT, and fluorescence analyses.

Compounds 1–3 in Scheme 1 were synthesized according to the reported methods [25]. The obtained compound 3 (0.029 g, 0.50 mmol) and 2,4-dihydroxybenzaldehyde (0.138 g, 1.00 mmol) were dissolved in methanol (25 mL), and the mixture was stirred at room temperature for 6 h. When completed, the reaction mixture was concentrated in vacuo and subsequently purified by column chromatography (silica gel, V (dichloromethane): V (ethanol) = 300:1 as eluent) to afford the probe RCya.

Probe RCya: 0.210 g, green solid; yield 48.26%. ^1H NMR (400 MHz, CDCl_3) δ : 1.11 (s, 6H, $2\times\text{-CH}_3$), 1.43–1.46 (m, 6H, $2\times\text{-CH}_3$), 2.32 (s, 3H, -CH_3), 3.36 (t, J 3.5 Hz, 2H, $\text{-CH}_2\text{-}$), 3.55–3.61 (m, 6H, $2\times\text{-CH}_2\text{-}$, $2\times\text{-OH}$), 3.87–3.93 (m, 4H, $2\times\text{-CH}_2\text{-}$), 6.50–6.53 (m, 4H, $3\times\text{=CH-}$, Ar-H), 6.62 (d, J 7.0 Hz, 2H, Ar-H), 6.76 (d, J 8.7 Hz, 1H, Ar-H), 7.02 (d, J 7.5 Hz, 2H, Ar-H), 7.11 (d, J 7.9 Hz, 1H, Ar-H), 7.23 (t, J 7.4 Hz, 1H, Ar-H), 7.42 (d, J 8.0 Hz, 1H, Ar-H), 7.86 (d, J 7.2 Hz, 2H, Ar-H), 8.16 (d, J 7.8 Hz, 1H, Ar-H), 8.53 (d, J 8.8 Hz, 1H, Ar-H), 9.27 (d, J 7.5 Hz, 1H, Ar-H). IR (KBr pellet, ν/cm^{-1}): 3427 (ν_{OH}); 1742 ($\nu_{\text{C=O}}$); 1621 ($\nu_{\text{C=N}}$); 1516 ($\nu_{\text{C=C}}$); 1412 (σ_{OH}); 1326, 1214 ($\nu_{\text{C-O-C}}$). Elem. Anal.: calcd. for $\text{C}_{44}\text{H}_{44}\text{N}_4\text{O}_4$: C 76.28, H 6.40, N 8.09; found: C 76.43, H 6.60, N 8.15. HRMS (TOF, m/z): calcd. for $\text{C}_{44}\text{H}_{44}\text{N}_4\text{O}_4$ 692.3363; found $[\text{M}+\text{H}^+]$ = 693.3237.

4.3. Spectroscopic Analysis

Stock solutions (100 $\mu\text{mol L}^{-1}$) of probe RCya, Pd^{2+} , Sn^{2+} , Cu^{2+} , Ca^{2+} , Mg^{2+} , Cr^{3+} , Cd^{2+} , Co^{2+} , Ba^{2+} , Pb^{2+} , Ag^+ , Fe^{3+} , Fe^{2+} , Ni^{2+} , Al^{3+} , Zn^{2+} , Mn^{2+} , Na^+ and K^+ were prepared in EtOH- H_2O (V (EtOH): V (H_2O) = 1:99, PBS, pH = 7.4). When used for spectroscopic tests, the stock solutions were usually diluted with EtOH- H_2O (V (EtOH): V (H_2O) = 1:99, PBS, pH = 7.4) to 10 $\mu\text{mol L}^{-1}$ unless noted. All the measurements were performed at least in triplicate and averaged.

4.4. DFT Calculations

To evaluate the photo-induced luminescence process and verify the proposed mechanism of RCya–Pd²⁺ recognition, DFT calculations [26,27] were employed to construct the molecular model using 6–31G** for C/H elements, 6–31+G* for N/O/S elements, and DGDZVP for Pd on Gaussian 09 Program. The polarizable continuum model was applied to simulate the solution environment with ethanol as the solvent, and all the optimized structures were confirmed with no imaginary frequency.

4.5. Nanofiber Imaging

For the detection and imaging of Pd²⁺ by RCya on solid-state nanofibers, composite nanofibers that contained probe RCya and polyacrylonitrile (PAN $M_w = 30,000$, m (RCya): m (PAN) = 1:1000, DMF solution) as the matrix were prepared through the electrospinning technique. When used for nanofiber imaging, the RCya–PAN composite nanofibers were then immersed into a target ion-containing aqueous solution and imaged under ambient light or under the 365 nm ultraviolet lamp.

4.6. Cytotoxicity

Methyl Thiazolyl Tetrazolium (MTT) assay [28] was adopted to evaluate the toxicity of Pd²⁺ and RCya–Pd²⁺ in HeLa cells. HeLa cells in the exponential phase of growth were cultured in Dulbecco's Modified Eagle Medium (DMEM) with 10% Fetal Bovine Serum (FBS). After digested with 0.25% trypsin solution, cells were dispensed in 96-well cell culture clusters (200 μ L per well) at a density of 2.5×10^4 cells per mL, incubated at 37 °C with 5% CO₂ for 24 h. The probe RCya (100 mmol L⁻¹ in DMSO) was then added to the 96-well plates and incubated for another 24 h to achieve a concentration gradient [29] of 6.25, 12.50, 25.00, 50.00, and 100.00 μ mol L⁻¹. Subsequently, the medium was removed, the cells were washed with PBS three times and incubated with 5.0 mg mL⁻¹ MTT solution (20 μ L MTT and 180 μ L medium) at 37 °C for 4 h. After that, the cells were washed with PBS three times (1 mL per well) and then dissolved in DMSO (150 μ L per well). The optical intensity at 490 nm, conducted in triplicate, was recorded on a microplate spectrophotometer. Data were expressed as mean \pm standard deviation (SD).

4.7. Fluorescent Imaging in Living Cells

HeLa cells were cultured in 10% FBS-containing DMEM at 37 °C in the humidified atmosphere with 5% CO₂. After 2 h, the growth medium was removed, and the cells were firstly washed with DMEM and incubated with 10 μ mol L⁻¹ of probe RCya for 30 min at 37 °C, then washed three times with PBS and imaged [30,31]. After subsequently adding 10 μ mol L⁻¹ Pd²⁺, HeLa cells were finally incubated with RCya and Pd²⁺ for 30 min at 37 °C, washed three times with PBS, and imaged. In the co-staining experiments of RCya–Mito/Lyso, HeLa cells were costained with 1 μ mol L⁻¹ RCya, 1 μ mol L⁻¹ Pd²⁺, and 100 nmol L⁻¹ Mito/Lyso Tracker for 30 min at 37 °C, and then washed three times with PBS and imaged.

Author Contributions: Conceptualization and writing—review and editing, Z.C.; methodology and visualization, X.J. and X.Z.; validation and formal analysis, Z.C.; investigation, X.J.; resources, Y.L.; writing—original draft preparation, X.Z.; supervision, Z.C.; project administration, Z.C.; funding acquisition, Z.C. and X.Z. All authors have read and agreed to the published version of this manuscript.

Funding: This research was funded by the Natural Science Foundation of Shaanxi Provincial Department of Education (22JHQ075), Shaanxi Natural Science Basic Research Project (2022JM-542, 2021JM-502), Xi'an Science and Technology Plan Project (22GXFW0122), and Xi'an Association for Science and Technology Project (095920221366).

Institutional Review Board Statement: Not applicable.

Informed Consent Statement: Not applicable.

Data Availability Statement: The data presented in this study are available in the article.

Conflicts of Interest: The authors declare no conflict of interest.

Sample Availability: Samples of the compounds are available from the authors.

References

1. Lavado, L.K.; Zhang, M.H.; Patel, K.; Khan, S.; Patel, U.K. Biometals as Potential Predictors of the Neurodegenerative Decline in Alzheimer's Disease. *Cureus* **2019**, *11*, e5573. [[CrossRef](#)] [[PubMed](#)]
2. Jing, S.Q.; Wang, S.S.; Zhong, R.M.; Zhang, J.Y.; Wu, J.Z.; Pu, Y.; Yan, L.J. Neuroprotection of *Cyperus esculentus* L. orientin against cerebral ischemia/reperfusion induced brain injury. *Neural Regen. Res.* **2020**, *15*, 548–556. [[CrossRef](#)] [[PubMed](#)]
3. Jun, Y.W.; Cho, S.W.; Jung, J.; Huh, Y.; Kim, Y.; Kim, D.; Ahn, K.H. Frontiers in probing Alzheimer's Disease biomarkers with fluorescent small molecules. *ACS Cent. Sci.* **2019**, *5*, 209–217. [[CrossRef](#)] [[PubMed](#)]
4. Garrett, C.E.; Prasad, K. The Art of Meeting Palladium Specifications in Active Pharmaceutical Ingredients Produced by Pd-Catalyzed Reactions. *Adv. Synth. Catal.* **2004**, *346*, 889–900. [[CrossRef](#)]
5. Luo, W.; Li, J.; Liu, W. A two-photon ratiometric ESIPT probe for fast detection and bioimaging of palladium species. *Org. Biomol. Chem.* **2017**, *15*, 5846–5850. [[CrossRef](#)]
6. Wen, J.; Lv, Y.; Xia, P.; Liu, F.; Xu, Y.; Li, H.; Chen, S.S.; Sun, S. A water-soluble near-infrared fluorescent probe for specific Pd²⁺ detection. *Bioorg. Med. Chem.* **2018**, *26*, 931–937. [[CrossRef](#)]
7. Zhou, L.; Wang, Q.; Zhang, X.-B.; Tan, W. Through-bond energy transfer-based ratiometric two-photon probe for fluorescent imaging of Pd²⁺ ions in living cells and tissues. *Anal. Chem.* **2015**, *87*, 4503–4507. [[CrossRef](#)]
8. Luo, W.; Liu, W. A water-soluble colorimetric two-photon probe for discrimination of different palladium species and its application in bioimaging. *Dalton Trans.* **2016**, *45*, 11682–11687. [[CrossRef](#)]
9. Zhang, Y.-S.; Balamurugan, R.; Lin, J.-C.; Fitriyani, S.; Liu, J.H.; Emelyanenko, A. Pd²⁺ fluorescent sensors based on amino and imino derivatives of rhodamine and improvement of water solubility by the formation of inclusion complexes with β -cyclodextrin. *Analyst* **2017**, *142*, 1536–1544. [[CrossRef](#)]
10. Zhu, X.; Zhang, Z.; Xue, Z.; Huang, C.; Shan, Y.; Liu, C.; Qin, X.; Yang, W.; Chen, X.; Wang, T. Understanding the selective detection of Fe³⁺ based on graphene quantum dots as fluorescent probes: The K_{sp} of a metal hydroxide-assisted mechanism. *Anal. Chem.* **2017**, *89*, 12054–12058. [[CrossRef](#)]
11. Kuijpers, K.P.L.; Bottecchia, C.; Cambié, D.; Drummen, K.; König, N.J.; Noël, T. A fully automated continuous-flow platform for fluorescence quenching studies and Stern-Volmer analysis. *Angew. Chem. Int. Ed. Engl.* **2018**, *57*, 11278–11282. [[CrossRef](#)]
12. Song, Y.; Pruden, A.; Edwards, M.A.; Rhoads, W.J. Natural organic matter, orthophosphate, pH, and growth phase can limit copper antimicrobial efficacy for *legionella* in drinking water. *Environ. Sci. Technol.* **2021**, *55*, 1759–1768. [[CrossRef](#)]
13. Ning, J.; Wang, W.; Ge, G.; Chu, P.; Long, F.; Yang, Y.; Peng, Y.; Feng, L.; Ma, X.; James, T.D. Target enzyme-activated two-photon fluorescent probes: A case study of CYP3A4 using a two-dimensional design strategy. *Angew. Chem. Int. Ed. Engl.* **2019**, *58*, 9959–9963. [[CrossRef](#)]
14. Ning, J.; Liu, T.; Dong, P.; Wang, W.; Ge, G.; Wang, B.; Yu, Z.; Shi, L.; Tian, X.; Huo, X.; et al. Molecular design strategy to construct the near-infrared fluorescent probe for selectively sensing human cytochrome P450 2J2. *J. Am. Chem. Soc.* **2019**, *141*, 1126–1134. [[CrossRef](#)]
15. Varadaraju, C.; Paulraj, M.S.; Tamilselvan, G.; Enoch, I.V.M.V.; Srinivasadesikan, V.; Shyi-Long, L. Evaluation of metal ion sensing behaviour of fluorescent probe along with its precursors: PET-CHEF mechanism, molecular logic gate behaviour and DFT studies. *J. Incl. Phenom. Macrocycl. Chem.* **2019**, *95*, 79–89. [[CrossRef](#)]
16. Zhang, X.; Zhang, F.; Chai, J.; Yang, B.; Liu, B. A TICT+AIE based fluorescent probe for ultrafast response of hypochlorite in living cells and mouse. *Spectrochim. Acta A Mol. Biomol. Spectrosc.* **2021**, *256*, 119735. [[CrossRef](#)]
17. Seyedi, S.; Parvin, P.; Jafargholi, A.; Abbasian, A.; Mehdinejad, M.; Khorrami, A.; Mehrabi, M.; Moafi, A. Fluorescence emission quenching of RdB fluorophores in attendance of various blood type RBCs based on Stern-Volmer formalism. *Spectrochim. Acta A Mol. Biomol. Spectrosc.* **2021**, *248*, 119237. [[CrossRef](#)]
18. Lai, J.; Zhou, H.; Jin, Z.; Li, S.; Liu, H.; Jin, X.; Luo, C.; Ma, A.; Chen, W. Highly stretchable, fatigue-resistant, electrically conductive, and temperature-tolerant ionogels for high-performance flexible sensors. *ACS Appl. Mater. Interfaces* **2019**, *11*, 26412–26420. [[CrossRef](#)]
19. Zhou, L.; Hu, S.; Wang, H.; Sun, H.; Zhang, X. A novel ratiometric two-photon fluorescent probe for imaging of Pd²⁺ ions in living cells and tissues. *Spectrochim. Acta Part A* **2016**, *166*, 25–30. [[CrossRef](#)]
20. Hassan, S.A.E.; Ahmed, S.A.E.; Helmy, A.H.; Youssef, N.F. Spectrofluorimetric study on fluorescence quenching of tyrosine and l-tryptophan by the aniracetam cognition enhancer drug: Quenching mechanism using Stern-Volmer and double-log plots. *Luminescence* **2020**, *35*, 728–737. [[CrossRef](#)]
21. Toprak, M. Fluorescence study on the interaction of human serum albumin with Butein in liposomes. *Spectrochim. Acta Part A* **2016**, *154*, 108–113. [[CrossRef](#)] [[PubMed](#)]
22. Sun, Y.; Wei, S.; Zhao, Y.; Hu, X.; Fan, J. Characterization of the interaction between 4-(tetrahydro-2-furanmethoxy)-N-octadecyl-1,8-naphthalimide and human serum albumin by molecular spectroscopy and its analytical application. *Appl. Spectrosc.* **2012**, *66*, 464–469. [[CrossRef](#)] [[PubMed](#)]

23. Freixa, Z.; Rivilla, I.; Monrabal, F.; Gómez-Cadenas, J.J.; Cossío, F.P. Bicolour fluorescent molecular sensors for cations: Design and experimental validation. *Phys. Chem. Chem. Phys.* **2021**, *23*, 15440–15457. [[CrossRef](#)] [[PubMed](#)]
24. Tian, X.; Murfin, L.C.; Wu, L.; Lewis, S.E.; James, T.D. Fluorescent small organic probes for biosensing. *Chem. Sci.* **2021**, *12*, 3406–3426. [[CrossRef](#)] [[PubMed](#)]
25. Xie, J.-Y.; Li, C.-Y.; Li, Y.-F.; Fei, J.; Xu, F.; Ou-Yang, J.; Liu, J. Near-infrared fluorescent probe with high quantum yield and its application in the selective detection of glutathione in living cells and tissues. *Anal. Chem.* **2016**, *88*, 9746–9752. [[CrossRef](#)]
26. Sugi, Y.; Premkumar, S.; Joseph, S.; Ramadass, K.; Sathish, C.I.; Dasireddy, V.D.B.C.; Yang, J.-H.; Liu, Q.; Kuota, Y.; Vinu, A. Substitutional isomerism of triisopropyl naphthalenes in the isopropylation of naphthalene. Assignment by gas chromatography and confirmation by DFT calculation. *Res. Chem. Intermed.* **2022**, *48*, 869–884. [[CrossRef](#)]
27. Tian, M.; He, H.; Wang, B.B.; Wang, X.; Liu, Y.; Jiang, F.L. A reaction-based turn-on fluorescent sensor for the detection of Cu(II) with excellent sensitivity and selectivity: Synthesis, DFT calculations, kinetics and application in real water samples. *Dyes Pigm.* **2019**, *165*, 383–390. [[CrossRef](#)]
28. Savran, T.; Karuk Elmas, S.N.; Aydin, D.; Arslan, S.; Arslan, F.N.; Yilmaz, I. Design of multiple-target chemoprobe: “naked-eye” colorimetric recognition of Fe³⁺ and off-on fluorogenic detection for Hg²⁺ and its on-site applications. *Res. Chem. Intermed.* **2022**, *48*, 1003–1023. [[CrossRef](#)]
29. Li, S.; Zhao, B.; Kan, W.; Wang, L.; Song, B.; Chen, S. A off-on pH fluorescence probe derived from phenanthro[9,10-d]imidazol-fluorescein based on ES IPT and ICT. *Res. Chem. Intermed.* **2018**, *44*, 491–502. [[CrossRef](#)]
30. Palanisamy, S.; Wang, Y.L.; Chen, Y.J.; Chen, C.Y.; Tsai, F.T.; Liaw, W.F.; Wang, Y.M. In vitro and in vivo imaging of nitroxyl with copper fluorescent probe in living cells and zebrafish. *Molecules* **2018**, *23*, 2551. [[CrossRef](#)]
31. Yi, X.Q.; He, Y.F.; Cao, Y.S.; Shen, W.X.; Lv, Y.Y. Porphyrinic probe for fluorescence “turn-on” monitoring of Cu⁺ in aqueous buffer and mitochondria. *ACS Sens.* **2019**, *4*, 856–864. [[CrossRef](#)]

Disclaimer/Publisher’s Note: The statements, opinions and data contained in all publications are solely those of the individual author(s) and contributor(s) and not of MDPI and/or the editor(s). MDPI and/or the editor(s) disclaim responsibility for any injury to people or property resulting from any ideas, methods, instructions or products referred to in the content.